

Astro2020 Science White Paper

Hot Drivers of Stellar Feedback from 10 to 10,000 pc

Thematic Areas:

- Planetary Systems
- Star and Planet Formation
- Formation and Evolution of Compact Objects
- Cosmology and Fundamental Physics
- Stars and Stellar Evolution
- Resolved Stellar Populations and their Environments
- Galaxy Evolution
- Multi-Messenger Astronomy and Astrophysics

Principal Author:

Name: Edmund Hodges-Kluck
Institution: University of Maryland/NASA GSFC
Email: edmund.hodges-kluck@nasa.gov

Co-authors:

Laura A. Lopez (The Ohio State University), Mihoko Yukita (Johns Hopkins University/NASA GSFC), Andrew Ptak (NASA GSFC), Douglas Swartz (NASA MSFC/USRA), Panayiotis Tzanavaris (University of Maryland, Baltimore County/NASA GSFC), Sylvain Veilleux (University of Maryland), Joel Bregman (University of Michigan)

Abstract: Stellar feedback – stars regulating further star formation through the injection of energy and momentum into the interstellar medium – operates through a complex set of processes that originate in star clusters but shape entire galaxies. A mature theory of stellar feedback is essential to a complete theory of star and galaxy formation, but the energy and momentum injected by hot gas into its surroundings remains unclear. With a next-generation X-ray observatory, breakthrough progress can be made through precision measurements of the temperature, density, velocity, and abundances of hot gas on scales of star clusters to galactic superwinds.

1. The Importance of Stellar Feedback – and its Uncertainties

Stellar feedback – the injection of energy and momentum by stars into their environment – originates at the small scales of star clusters (<10 pc), yet shapes galaxies on large scales (>10 kpc); it is necessary for forming realistic galaxies in simulations^{1;2} and accounting for observed galaxy properties^{3;4;5}. Stellar feedback maintains the multi-phase structure of the interstellar medium (ISM)⁶, inefficient star formation^{7;8}, and the life-cycle of giant molecular clouds (GMCs)^{9;10}. Meanwhile, it generates hot gas, radiation, and cosmic rays that can expel gas from galaxies^{11;12}.

The nature of stellar feedback is the source of some of the largest uncertainties in star- and galaxy-formation models^{13;2}. For example, depending on how feedback is implemented, the properties of Milky Way-like galaxies at $z = 0$ can vary by orders of magnitude^{14;15}. These uncertainties stem primarily from four challenges: 1) the large dynamic range over which feedback is important; 2) the need to consider multiple modes of interconnected feedback; 3) the question of where energy and momentum are deposited; and 4) a dearth of observational constraints.

Recent “zoom-in” simulations on parsec scales^{16;17;18;2} are starting to overcome some of these issues by incorporating more relevant sub-grid physics. However, observations are essential for testing and improving these models. In particular, the role of hot ($\sim 10^7$ - 10^8 K) gas shock-heated by stellar winds and supernovae (SNe) remains unclear, on both the small scales of H II regions and on the large scales of galactic winds. Precise measurements of the energy, momentum, distribution, and metal content of the hot gas over four orders of magnitude in scale are needed to address these outstanding questions, and motivate the need for next-generation X-ray missions.

2. Feedback in Star Clusters (<10 pc)

Fast stellar winds and SNe carve out large cavities, called superbubbles, that sweep up material from the surrounding medium. Further, SNe within the bubble thermalize efficiently, and the bubble becomes filled with tenuous, hot ($\sim 10^7$ K), shock-heated gas^{19;20;21;22;23}. As the bubble expands, much of the energy is radiated away, but the remainder can disrupt cool clouds and inject turbulence into the ISM^{6;24}. This basic picture has been validated by observations: hot gas in bubbles detected by *Chandra* and *XMM-Newton*^{25;26} is consistent with models for superbubble expansion^{27;28}.

To take the next step and implement realistic superbubble models into feedback simulations requires understanding how superbubbles grow in different environments, and how the hot gas depends on the mass, metallicity, and ambient ISM density of the natal star cluster. These are not minor problems: studies of H II regions in the Milky Way and LMC find temperatures between $kT \approx 0.1$ - 0.8 keV ($T \approx 10^6$ - 10^7 K) and luminosities $L_X \sim 10^{31}$ - 10^{35} erg s⁻¹^{29;30;31}. The large dispersion in L_X reflects different severity of energy losses, e.g., from radiative and adiabatic cooling (depending on how much work the hot gas does on its surroundings), thermal conduction, dust heating, and leakage of hot gas through the H II shells³².

It is therefore insufficient to study just a few nearby H II regions in great detail. Instead, we need an inventory of hot gas in thousands of H II regions in the Local Group, providing L_X , kT , and Z/Z_\odot (or Z_{Fe} and Z_\odot). This is not feasible with *Chandra* or *XMM-Newton*. The main emission lines from gas at 10^6 - 10^7 K occur between 0.5-1 keV, where a collecting area $A_{\text{eff}} > 5,000$ cm² is needed to detect X-ray faint ($L_X \sim 10^{32}$ erg s⁻¹) superbubbles out to 1 Mpc (in <1 Ms exposures). Several hundred X-ray photons are needed to make basic measurements, so a large collecting area is essential. These requirements are met by *Athena*³³. With its higher angular resolution ($\theta \lesssim 0.5''$), the *Lynx* strategic mission³⁴ would extend this study to gas leaking out of bubbles.

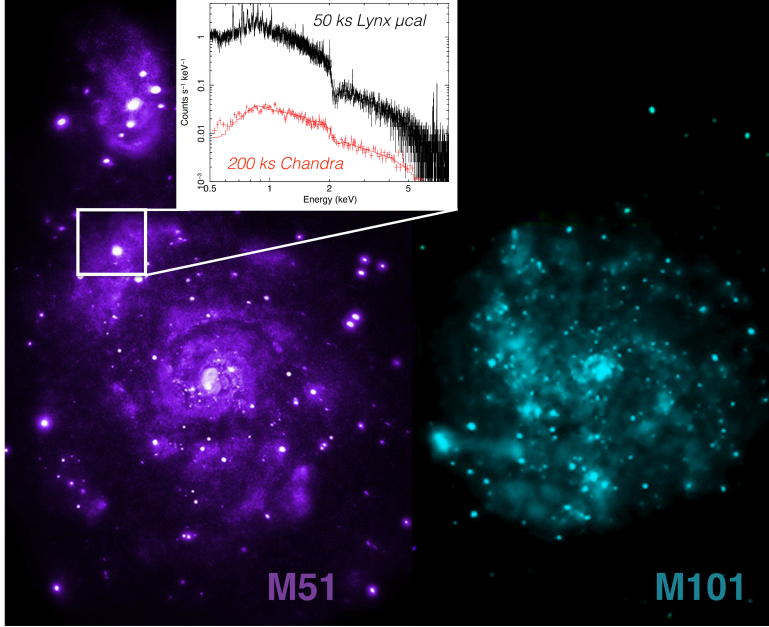


Fig. 1: *Chandra* images of M51 (left; 850 ks³⁶) and M101 (right; 1 Ms³⁵). The inset shows the 200 ks *Chandra* spectrum (red) of the diffuse gas from a 1' portion of the M51 disk. For comparison, a simulated spectrum (black, based on two thermal plasma models) from a 50-ks observation with the *Lynx* microcalorimeter is shown, which resolves emission lines from heavy elements (e.g., Si, Fe) in the ISM of M51. $\sim 1''$ spatial resolution across the entire galaxy is needed to detect and mask point sources, and thus obtain an accurate inventory of the hot gas energy.

Detecting brighter superbubbles with $L_X = 10^{33}$ - 10^{35} erg s⁻¹ in external galaxies requires high angular resolution ($\theta < 1''$, corresponding to 25 pc and 50 pc at 5 Mpc and 10 Mpc). Figure 1 shows what the hot ISM looks like with high resolution *Chandra* observations^{35;36}; superbubbles appear as faint knots (which are hard to distinguish visibly from the brighter X-ray binaries). These luminosities also require high sensitivity ($A_{\text{eff}} > 5,000$ cm² for a calorimeter) and a wide field of view (>15 arcmin) to efficiently accumulate a sample of hundreds to thousands of superbubbles.

3. Supernova Feedback from Star Clusters to Galaxies (10-1000 pc)

Hot gas in superbubbles compresses cooler gas, drives turbulence in the ISM, distributes metals, expels hot gas from the disk in fountain flows, and forms channels through which ionizing photons from young star clusters can escape the galaxy. These processes work in tandem with, and depend on, momentum injected by radiation pressure and cosmic rays. The energy and momentum of the hot ISM also depends on density, which controls radiative losses. Sophisticated simulations are needed to understand what happens after gas escapes from its home cluster.

Models are becoming less phenomenological and more physical: they include recipes for plasma heating and cooling, mixing of hot and cold gas, magnetic fields, stellar mass-loss, etc³⁷. However, the observational constraints on the hot ISM needed to inform these models remain poor. Important measurements include the thermalization efficiency of SNe (ϵ) as a function of environment^{38;39;40}, the mass-loading factor (β) in outflows^{41;42}, and the mass in hot gas as a function of temperature and density (a phase diagram). ϵ and β characterize the quantitative impact of outflows and momentum injection into the ISM, while the phase diagram globally constrains ISM models.

These quantities map to the temperature (kT) and density (n) of the hot plasma; for example, the temperature is proportional to the ratio ϵ/β , and β can be constrained with the radius of the hot region and the star-formation rate^{43;44;45}. These measurements are challenging to make because the X-ray luminosity is proportional to n^2 (requiring much longer exposures to measure n in tenuous regions, such as between spiral arms), and much of the X-ray emitting gas is not in collisional ionization equilibrium⁴⁶, so commonly used thermal plasma models are misleading.

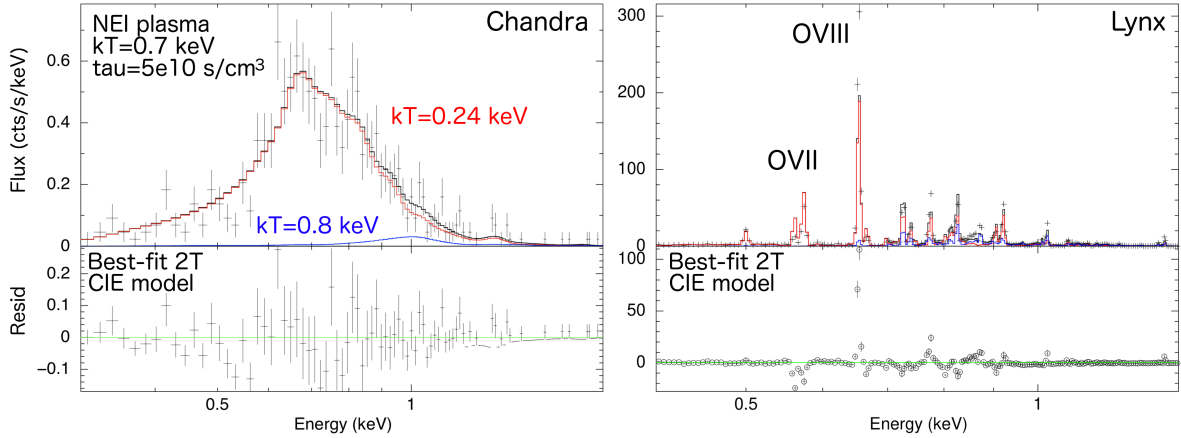


Fig. 2: Much of the X-ray bright ISM may not be in collisional ionization equilibrium (CIE), but high energy resolution is needed to properly model it. **Left:** A simulated non-equilibrium ionization (NEI) plasma model at CCD energy resolution (with $kT = 0.7$ keV and ionization timescale $\tau = 5 \times 10^{10}$ s cm $^{-3}$) is adequately fit by a CIE model with $kT_1 = 0.24$ keV and $kT_2 = 0.8$ keV. **Right:** When the main emission lines are resolved, no CIE model can possibly fit the data, as evidenced by a poor fit to the expected CIE line strengths.

Current observational data are completely unmatched to the scope of the problem. Outside of the Local Group, few galaxies have enough signal from hot gas to make any measurements on the spatial scales relevant to constraining simulations, and instead the hot ISM properties are inferred from a single spectrum from the whole galaxy. Even in the few cases with deep *Chandra* data (Figure 1), measurements on sub-kpc scales are hindered by low energy resolution, which makes it difficult to distinguish non-equilibrium and collisional equilibrium models (Figure 2). Indeed, this may be why the hot ISM in most star-forming galaxies can be fit by a two-temperature collisional plasma^{47;35;48} with $kT_1 \sim 0.1$ -0.2 keV and $kT_2 \sim 0.5$ -0.8 keV.

Accurate modeling of the hot ISM spectrum on scales of 0.1-1 kpc requires high angular resolution ($\theta < 1 - 10''$), a large collecting area ($A_{\text{eff}} > 2,000$ cm 2 at 1 keV) and energy resolution $\Delta E < 4$ eV. The *Athena* X-IFU meets these requirements for nearby galaxies. $\theta < 1 - 2''$ is needed to fully inventory the hot gas in galaxies within 30 Mpc.

Higher resolution ($\theta \lesssim 1''$) is needed to resolve the *interfaces* of hot and cool gas in detail beyond the Local Group. *Chandra* images reveal edges in the hot ISM related to stellar structure³⁶, magnetic fields, and filamentary structures⁴⁹ seen in other wavelengths, and studies of galaxy clusters and supernova remnants highlight the need to resolve edges to capture the essential physics (see the white paper by Markevitch et al.). This is generally feasible only with *Lynx*, although *Athena*, in tandem with existing *Chandra* data, will be able to study some nearby edges.

4. What Drives Galactic Winds? (100-10,000 pc)

Efficient thermalization of SNe in starburst galaxies forms pockets of superheated ($T > 10^8$ K) gas that break out of the disk and drive winds with hot component velocities $v_{\text{hot}} > 1000$ km s $^{-1}$ ^{43;50}. The hot wind contains more than 90% of the total wind energy and most of the metals⁵¹, but it may not be able to accelerate cool clouds (which dominate the wind mass) to the observed $v \lesssim 1000$ km s $^{-1}$ without shredding them, so alternative momentum sources such as cosmic rays and radiation pressure have been explored⁵². The question remains, *does* the hot wind couple to the mass (and *how*?) How does the wind evolve as it expands, and how many metals does it carry?

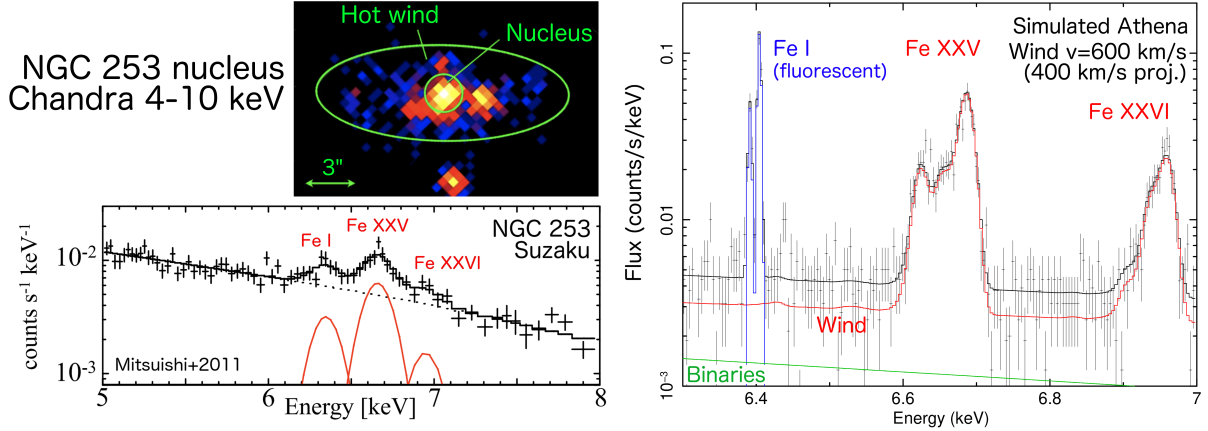


Fig. 3: **Left:** *Suzaku* detected diffuse hot gas in NGC 253 through Fe XXV and Fe XXVI lines⁵³, which however are unresolved, leading to a limit on v_{hot} . **Right:** A simulated *Athena* spectrum from the nucleus resolves the lines (Fe I $K\alpha$ is fluorescent and not from the hot wind). **The input line-of-sight velocity is recovered by centroiding to $\Delta v = 40 \text{ km s}^{-1}$ (10%), illustrating the power of a calorimeter.**

Understanding the hot wind begins with measuring its energy content, E_{wind} , which requires n , kT , and v_{hot} at the wind's base. Superheated gas has been detected in the nearby superwind galaxies M82^{44;54} and NGC 253⁵³ through diffuse Fe XXV emission (Figure 3), but the energy resolutions (ΔE) of existing spectrometers are too low to directly measure v_{hot} . To constrain v_{hot} to a precision of 25%, which limits the precision on E_{wind} , through line widths and centroids requires $\Delta E \leq 5 \text{ eV}$ at the 6.7 keV Fe XXV line (centroid accuracy is $\sim \Delta E / [S/N]$). The Resolve calorimeter on board *XRISM*¹ ($\Delta E = 5 \text{ eV}$, $\theta = 1.6'$) will do this for M82 and NGC 253. Line ratios within the Fe XXV and Fe XXVI complexes, using the same data, constrain n and kT .

The first measurements of v_{hot} will be a breakthrough, but will not tell us how E_{wind} relates to the star-formation rate, stellar mass, and metallicity. Strickland et al. (2009)⁵⁶ identified about 25 winds sufficiently bright to observe with modest exposure times (100-200 ks) for $A_{\text{eff}} \sim 1000\text{-}2000 \text{ cm}^2$. Isolating the superheated gas from bright X-ray binaries in the more distant galaxies requires angular resolution $\theta < 5''\text{-}10''$, while measuring E_{wind} to 10% requires $\Delta E \leq 2 \text{ eV}$.

A more ambitious goal that would connect the hot wind to its cooler surroundings (as measured with optical IFUs) involves *mapping* the velocities of diffuse Fe XXV and Fe XXVI. Based on *Chandra* images (e.g., Figure 3), this would require higher angular resolution ($\theta < 1''\text{-}2''$) and correspondingly larger A_{eff} for reasonable ($< 400 \text{ ks}$) exposures. Such measurements will be essential to understanding winds across cosmic time, as the underlying principles should be the same¹².

The fate of the hot wind is unclear. At larger radii, winds emit soft X-rays from 10^{6-7} K gas, which may result from radiative cooling⁵⁷ or shocked material¹¹. At least some of the emission comes from charge exchange (3-87% of the flux in strong lines^{45;58}). Models make predictions⁵² that can be tested with an X-ray calorimeter: in a radiatively cooling wind, kT would drop rapidly with height and v would drop gently⁵⁷. On the other hand, shocked clouds would not (necessarily) decline in either temperature or velocity with radius. We need to measure the velocity of the 10^{6-7} K gas to 20-30%, using lines such as Mg XVII ($E = 1.47 \text{ keV}$, $T_{\text{peak}} = 10^7 \text{ K}$) and Ne X ($E = 1.02 \text{ keV}$, $T_{\text{peak}} = 5 \times 10^6 \text{ K}$). n and kT can be estimated from the He-like triplets in the 0.3–3 keV bandpass. These observations will also enable an inventory of the metal abundances in the hot gas.

¹The JAXA/NASA X-ray Imaging and Spectroscopy Mission⁵⁵, to replace *Hitomi* in 2022.

XRISM can resolve several winds, but a factor of 10 better θ and A_{eff} are needed for a sample⁵⁶. Even higher resolution is needed to move beyond phenomenology to understand the coupling of wind energy to cool gas in filaments, as soft X-ray winds are highly structured and may cool to form the warm filaments^{57:59}. Measuring velocities to 10-20% in the 10^6 - 10^7 keV gas and mapping abundances in individual filaments requires $\theta < 1''$, high spectral resolution ($\Delta E < 0.5$ eV, for lines at $E < 1$ keV), and $A_{\text{eff}} > 10,000$ cm². X-ray absorption (i.e., using gratings) is also a promising way to study these winds. This rich topic is explored in the white paper by Tremblay et al.

5. Winds and the Hot ISM out to $z \sim 1$

X-ray surveys to detect the most distant black holes are presented in other white papers, and the cameras needed to perform them (i.e., with $\theta \approx 1''$ across a $15'$ field of view) can also detect bright winds – and even the hot ISM – at cosmological distances. ULIRG winds, such as in NGC 6240 or Arp 220, are bright enough to detect up to $z \sim 1$, if the wind can be resolved ($1''$ at $z = 1.0$ corresponds to 8 kpc). The hot ISM is fainter, but could be resolved from X-ray binaries out to $z \sim 0.1$ in surveys, and to much larger distances ($z \sim 3$) in strongly lensed galaxies⁶⁰. The spectrum would recover the global temperature, density, and metallicity, subject to the caveats noted above.

6. Instrumental Requirements

Here we summarize the capabilities needed to execute an ambitious program that will transform our understanding of stellar feedback from small (< 10 pc) to large ($> 10,000$ pc) scales. This will require high angular resolution coupled with high spectral resolution, such as what can be attained with a micro-calorimeter in a high throughput observatory.

Science Goals	Methodology	Required Capabilities
Constrain how feedback properties vary as a function of star cluster mass, galactic environment, and metallicity	Characterize hot gas in thousands of HII regions in the Local Group and in superbubbles up to 30 Mpc	A_{eff} : 5,000 cm ² @ 1 keV θ : $< 10''$ (LG) θ : $0.5'' - 1.0''$ FoV: $\sim 15' \times 15'$
Constrain ϵ and β on 100-2,000 pc scales and in different environments and galaxies	Measure the temperature and density of hot gas in galaxies up to 30 Mpc	A_{eff} : 2,000 cm ² @ 1 keV θ : $1'' - 10''$ ΔE : < 4 eV
Measure the velocity and energy of the hot wind	Measure velocity of hot wind via the 6.7 keV Fe XXV line in ~ 25 nearby starbursts	A_{eff} : 2,000 cm ² @ 6 keV θ : $10''$ ΔE : < 2 eV
	Map the velocities of diffuse Fe XXV and Fe XXVI	A_{eff} : 3,000 cm ² @ 6 keV θ : $1 - 2''$ ΔE : $< 3 - 4$ eV
Understand the origin of the soft X-rays from galactic winds, and measure metal mass	Measure the velocity, temperature, and abundances as a function of wind radius in 20-30 systems	A_{eff} : 2,000 cm ² @ 1 keV θ : $3 - 20''$ ΔE : < 2 eV θ : $0.5''$ (filaments) ΔE : 0.5 eV (filaments)
Measure hot gas in and around galaxies to $z \sim 1$	Measure Wind/ISM temperature, density, and metallicity	A_{eff} : 5,000 cm ² @ 0.5 keV θ : $< 1''$ FoV: $\sim 15' \times 15'$

References

- [1] White, S. D. M. & Rees, M. J. Core condensation in heavy halos - A two-stage theory for galaxy formation and clustering. *MNRAS* **183**, 341–358 (1978).
- [2] Hopkins, P. F. *et al.* Galaxies on FIRE (Feedback In Realistic Environments): stellar feedback explains cosmologically inefficient star formation. *MNRAS* **445**, 581–603 (2014).
- [3] Kennicutt, R. C., Jr. The Global Schmidt Law in Star-forming Galaxies. *ApJ* **498**, 541–552 (1998).
- [4] Tremonti, C. A. *et al.* The Origin of the Mass-Metallicity Relation: Insights from 53,000 Star-forming Galaxies in the Sloan Digital Sky Survey. *ApJ* **613**, 898–913 (2004).
- [5] Muratov, A. L. *et al.* Gusty, gaseous flows of FIRE: galactic winds in cosmological simulations with explicit stellar feedback. *MNRAS* **454**, 2691–2713 (2015).
- [6] McKee, C. F. & Ostriker, J. P. A theory of the interstellar medium - Three components regulated by supernova explosions in an inhomogeneous substrate. *ApJ* **218**, 148–169 (1977).
- [7] Zuckerman, B. & Evans, N. J., II. Models of massive molecular clouds. *ApJ* **192**, L149–L152 (1974).
- [8] Krumholz, M. R. & Tan, J. C. Slow Star Formation in Dense Gas: Evidence and Implications. *ApJ* **654**, 304–315 (2007).
- [9] Matzner, C. D. On the Role of Massive Stars in the Support and Destruction of Giant Molecular Clouds. *ApJ* **566**, 302–314 (2002).
- [10] Krumholz, M. R., Matzner, C. D. & McKee, C. F. The Global Evolution of Giant Molecular Clouds. I. Model Formulation and Quasi-Equilibrium Behavior. *ApJ* **653**, 361–382 (2006).
- [11] Veilleux, S., Cecil, G. & Bland-Hawthorn, J. Galactic Winds. *ARA&A* **43**, 769–826 (2005).
- [12] Heckman, T. M. & Thompson, T. A. A Brief Review of Galactic Winds. *arXiv e-prints* (2017).
- [13] Dobbs, C. L., Bonnell, I. A. & Pringle, J. E. The formation of molecular clouds in spiral galaxies. *MNRAS* **371**, 1663–1674 (2006).
- [14] Kim, J.-h. *et al.* The AGORA High-resolution Galaxy Simulations Comparison Project. *ApJS* **210**, 14 (2014).
- [15] Scannapieco, C. *et al.* The Aquila comparison project: the effects of feedback and numerical methods on simulations of galaxy formation. *MNRAS* **423**, 1726–1749 (2012).
- [16] Agertz, O., Kravtsov, A. V., Leitner, S. N. & Gnedin, N. Y. Toward a Complete Accounting of Energy and Momentum from Stellar Feedback in Galaxy Formation Simulations. *ApJ* **770**, 25 (2013).

- [17] Renaud, F. *et al.* A sub-parsec resolution simulation of the Milky Way: global structure of the interstellar medium and properties of molecular clouds. *MNRAS* **436**, 1836–1851 (2013).
- [18] Ceverino, D. *et al.* Radiative feedback and the low efficiency of galaxy formation in low-mass haloes at high redshift. *MNRAS* **442**, 1545–1559 (2014).
- [19] Castor, J., McCray, R. & Weaver, R. Interstellar bubbles. *ApJ* **200**, L107–L110 (1975).
- [20] Weaver, R., McCray, R., Castor, J., Shapiro, P. & Moore, R. Interstellar bubbles. II - Structure and evolution. *ApJ* **218**, 377–395 (1977).
- [21] Chu, Y.-H. & Mac Low, M.-M. X-rays from superbubbles in the Large Magellanic Cloud. *ApJ* **365**, 510–521 (1990).
- [22] Silich, S., Tenorio-Tagle, G. & Añorve-Zeferino, G. A. On the X-Ray Emission from Massive Star Clusters and Their Evolving Superbubbles. *ApJ* **635**, 1116–1125 (2005).
- [23] Rogers, H. & Pittard, J. M. Feedback from winds and supernovae in massive stellar clusters - II. X-ray emission. *MNRAS* **441**, 964–982 (2014).
- [24] Hopkins, P. F., Quataert, E. & Murray, N. The structure of the interstellar medium of star-forming galaxies. *MNRAS* **421**, 3488–3521 (2012).
- [25] Townsley, L. K. *et al.* A Chandra ACIS Study of 30 Doradus. I. Superbubbles and Supernova Remnants. *AJ* **131**, 2140–2163 (2006).
- [26] Güdel, M. *et al.* Million-Degree Plasma Pervading the Extended Orion Nebula. *Science* **319**, 309 (2008).
- [27] Harper-Clark, E. & Murray, N. One-Dimensional Dynamical Models of the Carina Nebula Bubble. *ApJ* **693**, 1696–1712 (2009).
- [28] Wareing, C. J., Pittard, J. M., Wright, N. J. & Falle, S. A. E. G. A new mechanical stellar wind feedback model for the Rosette Nebula. *MNRAS* **475**, 3598–3612 (2018).
- [29] Chu, Y.-H., Chang, H.-W., Su, Y.-L. & Mac Low, M.-M. X-Rays from Superbubbles in the Large Magellanic Cloud. III. X-Ray–dim Superbubbles. *ApJ* **450**, 157 (1995).
- [30] Oey, M. S. The Dynamics of Superbubbles in the Large Magellanic Cloud. *ApJ* **467**, 666 (1996).
- [31] Jaskot, A. E., Strickland, D. K., Oey, M. S., Chu, Y.-H. & García-Segura, G. Observational Constraints on Superbubble X-ray Energy Budgets. *ApJ* **729**, 28 (2011).
- [32] Rosen, A. L., Lopez, L. A., Krumholz, M. R. & Ramirez-Ruiz, E. Gone with the wind: Where is the missing stellar wind energy from massive star clusters? *MNRAS* **442**, 2701–2716 (2014).
- [33] Barret, D. *et al.* The Athena X-ray Integral Field Unit (X-IFU). In *Space Telescopes and Instrumentation 2016: Ultraviolet to Gamma Ray*, vol. 9905 of *Proc. SPIE*, 99052F (2016). [astro-ph/1608.08105](https://arxiv.org/abs/astro-ph/1608.08105).

- [34] Gaskin, J. A. *et al.* The Lynx X-ray Observatory: concept study overview and status. In *Space Telescopes and Instrumentation 2018: Ultraviolet to Gamma Ray*, vol. 10699 of *Society of Photo-Optical Instrumentation Engineers (SPIE) Conference Series*, 106990N (2018).
- [35] Kuntz, K. D. & Snowden, S. L. The Chandra M101 Megasecond: Diffuse Emission. *ApJS* **188**, 46–74 (2010).
- [36] Kuntz, K. D., Long, K. S. & Kilgard, R. E. A Deep Chandra ACIS Survey of M51. *ApJ* **827**, 46 (2016).
- [37] Dale, J. E. The modelling of feedback in star formation simulations. *New Astr. Rev.* **68**, 1–33 (2015).
- [38] Hopkins, P. F., Narayanan, D. & Murray, N. The meaning and consequences of star formation criteria in galaxy models with resolved stellar feedback. *MNRAS* **432**, 2647–2653 (2013).
- [39] Vasiliev, E. O., Nath, B. B. & Shchekinov, Y. Evolution of multiple supernova remnants. *MNRAS* **446**, 1703–1715 (2015).
- [40] Fierlinger, K. M. *et al.* Stellar feedback efficiencies: supernovae versus stellar winds. *MNRAS* **456**, 710–730 (2016).
- [41] Zhang, D., Thompson, T. A., Murray, N. & Quataert, E. Hot Galactic Winds Constrained by the X-Ray Luminosities of Galaxies. *ApJ* **784**, 93 (2014).
- [42] Kim, C.-G. & Ostriker, E. C. Numerical Simulations of Multiphase Winds and Fountains from Star-forming Galactic Disks. I. Solar Neighborhood TIGRESS Model. *ApJ* **853**, 173 (2018).
- [43] Chevalier, R. A. & Clegg, A. W. Wind from a starburst galaxy nucleus. *Nature* **317**, 44 (1985).
- [44] Strickland, D. K. & Heckman, T. M. Supernova Feedback Efficiency and Mass Loading in the Starburst and Galactic Superwind Exemplar M82. *ApJ* **697**, 2030–2056 (2009).
- [45] Zhang, S. *et al.* Spectral Modeling of the Charge-exchange X-Ray Emission from M82. *ApJ* **794**, 61 (2014).
- [46] de Avillez, M. A. & Breitschwerdt, D. Time-dependent Cooling in Astrophysical Plasmas: The Non-equilibrium Ionization Structure of the Interstellar Medium and X-Ray Emission at Low Temperatures. *ApJ* **756**, L3 (2012).
- [47] Strickland, D. K., Heckman, T. M., Colbert, E. J. M., Hoopes, C. G. & Weaver, K. A. A High Spatial Resolution X-Ray and H α Study of Hot Gas in the Halos of Star-forming Disk Galaxies. I. Spatial and Spectral Properties of the Diffuse X-Ray Emission. *ApJS* **151**, 193–236 (2004).
- [48] Li, J.-T. & Wang, Q. D. Chandra survey of nearby highly inclined disc galaxies - I. X-ray measurements of galactic coronae. *MNRAS* **428**, 2085–2108 (2013).

- [49] Wang, Q. D., Immler, S., Walterbos, R., Lauroesch, J. T. & Breitschwerdt, D. Chandra Detection of a Hot Gaseous Corona around the Edge-on Galaxy NGC 4631. *ApJ* **555**, L99–L102 (2001).
- [50] Fielding, D., Quataert, E., Martizzi, D. & Faucher-Giguère, C.-A. How supernovae launch galactic winds? *MNRAS* **470**, L39–L43 (2017).
- [51] Strickland, D. K. & Stevens, I. R. Starburst-driven galactic winds - I. Energetics and intrinsic X-ray emission. *MNRAS* **314**, 511–545 (2000).
- [52] Zhang, D. A Review of the Theory of Galactic Winds Driven by Stellar Feedback. *Galaxies* **6**, 114 (2018).
- [53] Mitsuishi, I., Yamasaki, N. Y. & Takei, Y. Fe K Line Complex in the Nuclear Region of NGC 253. *ApJ* **742**, L31 (2011).
- [54] Liu, J., Gou, L., Yuan, W. & Mao, S. Fe K lines in the nuclear region of M82. *MNRAS* **437**, L76–L80 (2014).
- [55] Tashiro, M. *et al.* Concept of the X-ray Astronomy Recovery Mission. In *Space Telescopes and Instrumentation 2018: Ultraviolet to Gamma Ray*, vol. 10699 of *Society of Photo-Optical Instrumentation Engineers (SPIE) Conference Series*, 1069922 (2018).
- [56] Strickland, D. K. *et al.* Starburst Galaxies: Outflows of Metals and Energy into the IGM. In *astro2010: The Astronomy and Astrophysics Decadal Survey*, vol. 2010 of *Astronomy* (2009). [0902.2945](#).
- [57] Thompson, T. A., Quataert, E., Zhang, D. & Weinberg, D. H. An origin for multiphase gas in galactic winds and haloes. *MNRAS* **455**, 1830–1844 (2016).
- [58] Cumbee, R. S. *et al.* Ne X X-ray emission due to charge exchange in M82. *MNRAS* **458**, 3554–3560 (2016).
- [59] Schneider, E. E., Robertson, B. E. & Thompson, T. A. Production of Cool Gas in Thermally Driven Outflows. *ApJ* **862**, 56 (2018).
- [60] Dye, S. *et al.* Revealing the complex nature of the strong gravitationally lensed system H-ATLAS J090311.6+003906 using ALMA. *MNRAS* **452**, 2258–2268 (2015).